CONJUGATE NUMERICAL INVESTIGATION OF A MINIATURE FLAT-PLATE EVAPORATOR OF A CAPILLARY PUMPED LOOP FOR ELECTRONICS COOLING

ZHONGMIN WAN[1], WEI LIU[1], ZHENGKAI TU[1]
AND AKIRA NAKAYAMA[2]

[1] *College of Energy and Power Engineering,*
Huazhong University of Science and Technology,
Wuhan, 430074, P.R. China
zhongminwan@hotmail.com

[2] *Department of Mechanical Engineering, Shizuoka University,*
3-5-1 Johoku, Hamamatsu, 432-8561, Japan

(Received 22 March 2007)

Abstract: A capillary pumped loop (CPL) is a two-phase thermal control device applied in cooling electronic devices. A two-dimensional conjugate numerical model of a miniature flat-plate capillary evaporator is presented in order to describe liquid and vapor flow, heat transfer and phase change in the porous wick structure, liquid flow and heat transfer in the compensation cavity and heat transfer in the vapor grooves and the metallic wall. The entire evaporator is solved with the SIMPLE algorithm as a conjugate problem. The shape and location of the vapor-liquid interface inside the wick are calculated, and a side wall effect heat transfer limit is introduced to estimate the evaporator's heat transport capability. The influence of various wall materials on the evaporator's performance is discussed in detail. The results suggest that an evaporator with a combined wall is capable of dissipating high heat flux and stabilizing the temperature of electronic devices at a moderate temperature level.

Keywords: capillary pumped loop, flat-plate evaporator, side wall effect heat transfer limit, cooling of electronic devices

Notation

c – specific heat [$\mathrm{J\,kg^{-1}K^{-1}}$],
k – thermal conductivity [$\mathrm{W\,m^{-1}K^{-1}}$],
T – temperature [°C],
t – time [s],
$\vec{V}$ – velocity vector [$\mathrm{m\,s^{-1}}$],
P – pressure [Pa],
ΔP_c – capillary force [Pa],

K – permeability [m^2],
L_x – total length in the x direction [m],
L_{x1} – distance between the origin and the left surface of the wick [m],
L_{x2} – distance between the origin and the left surface of the compensation cavity [m],
L_{x3} – length of the bottom metallic wall [m],
L_y – total height in the y direction [m],
L_{y1} – height of the bottom metallic wall [m],
L_{y2} – height of the bottom surface of the wick [m],
L_{y3} – height of the upper surface of the wick [m],
q – heat flux [Wm^{-2}],
u – velocity in the x direction [ms^{-1}],
v – velocity in the y direction [ms^{-1}],
h_{fg} – latent heat of evaporation [Jkg^{-1}],
r_e – effective capillary radius of wick pores [m].

Greek symbols

μ – viscosity [Pas],
ρ – density [kgm^{-3}],
ε – porosity [%],
σ – liquid-vapor surface tension [Nm^{-1}],
θ – effective contact angle.

Subscripts

mw – metallic wall,
eff – effective,
l – liquid,
s – solid,
v – vapor,
in – inlet,
sat – saturation,
sub – subcooling,
sup – superheating,
al – aluminum,
st – stainless steel.

1. Introduction

The development trend of electronic devices is towards miniaturization, high power density and high performance quality. As the conventional heat transfer method of forced air convection is reaching its thermal limit [1, 2], the challenge is to develop alternative efficient cooling methods for high flux devices. A capillary pumped loop (CPL) is a two-phase thermal control device advanced in the last twenty years [3–5]. Because of its several advantages in terms of high heat transport capability, passive transport of heat over large distances with minimal temperature losses the use of capillary action for fluid transport and flexible transport lines, miniature CPL's have become a possible cooling choice in electronics. As a flat-plate evaporator has the advantages of perfect thermal contact between the surfaces of the evaporator and the

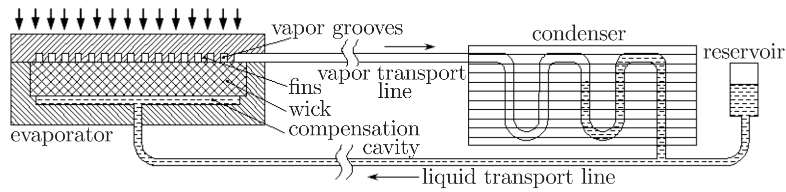

Figure 1. Schema of a miniature flat-plate CPL

electronic devices, low thermal resistance and isothermal heated surface, miniature flat-plate CPL's are considered a promising cooling method for dissipating increasingly higher power densities.

Figure 1 is a schematic diagram of a miniature flat-plate CPL for cooling in electronics, which consists of an evaporator, a condenser, a reservoir and vapor and liquid transport lines. Heat generated from electronic devices is applied to the evaporator, causing evaporation of the working fluid. A meniscus forms at the vapor-liquid interface in the evaporator's capillary structure and naturally adjusts itself to establish a capillary force matching the total pressure loss in the CPL system. The resulting vapor flows through the vapor grooves and vapor transport lines into the condenser, where it is condensed into liquid. The liquid condensate continues to flow through the liquid transport lines and returns to the evaporator, thus completing the cycle. The capillary evaporator is the most important part of a CPL system, as it is the heat absorbing element providing the capillary force of fluid flow through the loop. Heat generated from electronic devices in limited space can be effectively transported to a heat sink over long distances by flexible transport lines, and thus the problem of spatial limitations of electronic devices can be solved. The two-phase reservoir is used to control the temperature of the loop and accommodates fluid inventory shifts during changes under varying operating conditions.

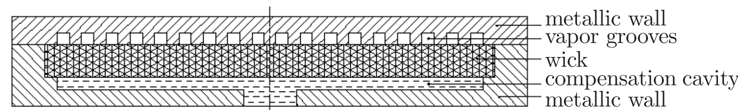

Figure 2. Schema of a miniature flat-plate evaporator

Although CPL's have become candidates for electronic cooling applications, the progress in reducing their evaporators' size to dimensions required for electronic applications has been slow, mainly due to insufficient understanding of the physical processes occurring there. Cao and Faghri [6] developed an analytical solution for the heat and mass transfer processes during evaporation in the wick of a CPL evaporator. It was assumed in their study that the entire porous structure was saturated with liquid and that the liquid-vapor interface was located in the unheated portion of the upper surface. Under these assumptions, only the liquid flow in the porous media needed to be studied and the capillary pressure at the liquid-vapor interface was neglected. In the same year, Demidov and Yatsenko [7] presented a numerical study showing that vapor zones can occur in the wick of the capillary evaporator under the fins. Figus *et al.* [8] offered a numerical solution for heat and mass transfer in a cylindrical evaporator wick using the Darcy model and a two-dimensional pore

network model. An important conclusion of this work was that the pore network model results were nearly identical to those of the Darcy model for ordered single pore-size distribution. Yan and Ochterbeck [9] provided a numerical study on the flow and heat transfer in the wick structure of an evaporator of a CPL based on the two-phase mixture model. The computational domain explored in the above-mentioned works was a single segment of an evaporator's wick structure. However, for a flat-plate CPL as shown in Figure 2, the capillary evaporator consists of a wick structure, a metallic wall, vapor grooves and a compensation cavity. The above-mentioned computational domain is merely a small part of the wick, which leads to limitations in evaluating the overall evaporator's performance with these models. Firstly, these models did not predict the influence of the metallic wall, the vapor grooves and the compensation cavity on the heat and mass transfer. Neither could the heated surface's temperature be obtained, very important in estimating the performance of thermal management systems of electronic devices. At the same time, the heat conduction of the metallic wall was neglected, which is inappropriate when studying the global evaporator performance, especially that of a miniature flat-plate CPL evaporator. Compared with the length of the heated surface, the thickness of the metallic side wall cannot be neglected. Due to the wall's high thermal conductivity, the liquid at the bottom of the wick and in the compensation cavity may heat up to a temperature exceeding the saturation temperature corresponding to the local saturation pressure by the wall's heat conduction. Vapor may be generate there, the presence of which has been found to block liquid flow to the vapor-liquid interface partially or fully [10], which may eventually lead to the evaporator getting dry and a failure of the CPL system. Therefore, a global model is indispensable for understanding the behavior of the capillary evaporator as a whole.

In the present work, a global capillary evaporator model of a miniature flat-plate CPL is presented which combines liquid and vapor flow, heat transfer and phase change in the porous wick structure, heat transfer and flow in the compensation cavity and heat transfer in the metallic wall. The entire evaporator is solved numerically with the SIMPLE algorithm as a conjugate problem. To the best of the authors' knowledge, no global evaporator model has been proposed before in the context of capillary evaporators.

2. Mathematical model

As the evaporator is assumed to be symmetric, a half of its cross-section is selected as the computational domain, as shown in Figure 3. The origin of the coordinate system is located in the bottom left corner of the evaporator.

The following main assumptions have been made in order to develop the mathematical model:

(1) the vapor flow in the vapor grooves is neglected for the sake of simplicity, so that heat transfer is mainly by conduction;
(2) the porous medium is rigid, homogenous, isotropic and fully saturated with fluid. There is local thermodynamic equilibrium between the solid phase and the liquid or vapor phase;
(3) the fluid is incompressible and has constant properties.

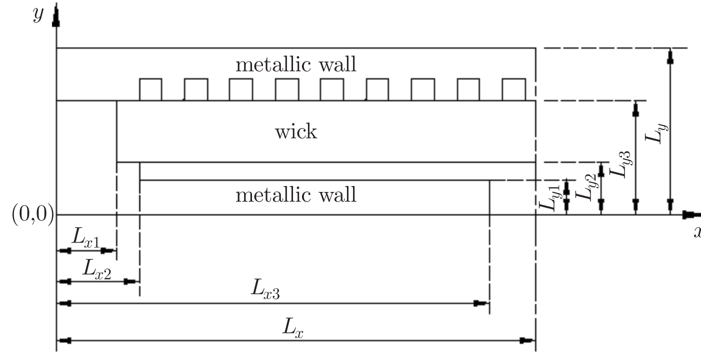

Figure 3. The computation domain and the coordinate system

The effect of gravity is neglected, and the heat and mass transfer in the liquid and vapor regions of the wick structure is based on the volume-averaged technique and the Brinkman-Darcy-Forchheimer model of porous media.

The governing equations of the global evaporator can be written as follows:

(1) metallic wall

$$(\rho c)_{mw}\frac{\partial T}{\partial t}=k_{mw}(\frac{\partial^2 T}{\partial x^2}+\frac{\partial^2 T}{\partial y^2}); \tag{1}$$

(2) vapor grooves

$$(\rho c)_{v}\frac{\partial T}{\partial t}=k_{v}(\frac{\partial^2 T}{\partial x^2}+\frac{\partial^2 T}{\partial y^2}); \tag{2}$$

(3) wick structure

continuum equation:

$$\frac{\partial(\varepsilon_i\rho_i)}{\partial t}+\nabla\cdot(\rho_i\vec{V}_i)=0; \tag{3}$$

momentum equation:

$$\frac{\rho_i}{\varepsilon_i}\frac{\partial\vec{V}_i}{\partial t}+\frac{\rho_i}{\varepsilon_i^2}\nabla(\vec{V}_i\cdot\nabla)\vec{V}_i=-\nabla p-\left(\frac{\mu_i}{K}+\frac{C}{\sqrt{K}}\right)|\vec{V}_i|\vec{V}_i+\frac{\mu_i}{\varepsilon_i}\nabla^2\vec{V}_i; \tag{4}$$

energy equation:

$$\overline{(\rho c)}_i\frac{\partial T}{\partial t}+\rho_i c_i(\vec{V}_i\cdot\nabla)T=(k_{eff})_i\nabla^2 T; \tag{5}$$

(4) compensation cavity

continuum equation:

$$\frac{\partial\rho_l}{\partial t}+\nabla\cdot(\rho_l\vec{V}_l)=0; \tag{6}$$

momentum equation:

$$\rho_l\frac{\partial\vec{V}_l}{\partial t}+\rho_l\nabla(\vec{V}_l\cdot\nabla)\vec{V}_l=-\nabla p+\mu_l\nabla^2\vec{V}_l; \tag{7}$$

energy equation:

$$\rho_l c_l\frac{\partial T}{\partial t}+\rho_l c_l(\vec{V}_l\cdot\nabla)T=k_l\nabla^2 T. \tag{8}$$

In the above equations $i=l,v$, C is the Forchheimer constant, n is the normal unit vector at the vapor-liquid interface, (k_{eff}) is the effective thermal conductivity,

$(k_{eff})_i = \varepsilon k_i + (1-\varepsilon)k_s$, $\overline{(\rho c)}$ is the density-capacity heat product defined in the energy equations, $\overline{(\rho c)}_i = \varepsilon\rho_i c_i + (1-\varepsilon)\rho_s c_s$.

Heat transfer in these regions is coupled, and the conservation equations must be solved as a conjugate problem. The boundary conditions of energy and momentum equations are given below:

– boundary conditions for energy equations

$$\text{at } x=0 \text{ or at } y=0: \quad k_{mw}\frac{\partial T}{\partial x} = h(T-T_a); \tag{9}$$

$$\text{at } x=L_x: \quad \frac{\partial T}{\partial x} = 0; \tag{10}$$

$$\text{at } y=L_y: \quad k_{mw}\frac{\partial T}{\partial y} = q; \tag{11}$$

– boundary conditions for momentum equations – due to fluid flow occurring mainly inside the wick structure and in the compensation cavity, the boundary conditions of momentum equations are as follows:

$$\text{at } y=0: \quad u_l=0, \quad v_l=0 \qquad 0\le x\le L_{x3}, \tag{12}$$

$$u_l=0, \quad v_l=v_{in} \qquad L_{x3}\le x\le L_x; \tag{13}$$

$$\text{at } y=L_{y3}: \quad \frac{\partial v_v}{\partial y}=0, \quad \frac{\partial u_v}{\partial x}+\frac{\partial v_v}{\partial y}=0 \quad \text{for the wick-vapor grooves border in the vapor phase region,} \tag{14}$$

$$u_i=0, \quad v_i=0 \quad \text{for other borders, } i=v,l; \tag{15}$$

$$\text{at } x=0 \text{ and } 0\le y\le L_{y3}: \quad u_i=0, \quad v_i=0 \qquad i=v,l; \tag{16}$$

$$\text{at } x=L_x \text{ and } 0\le y\le L_{y3}: \quad u_i=0, \quad \frac{\partial v_i}{\partial x}=0 \qquad i=v,l. \tag{17}$$

The inlet liquid velocity, v_{in}, of Equation (13) at the wick-compensation cavity border can be obtained by performing overall energy balancing on the capillary evaporator:

$$\rho_l\, v_{in}\,(L_x-L_{x3})(h_{fg}+c_l\Delta T_{sub}+c_v\Delta T_{sup})+Q_h = qL_x. \tag{18}$$

The left side of Equation (18) represents the heat absorbed by the working fluid and heat Q_h dissipated in the evaporator through heat convection. The right side of Equation (18) describes the heat applied at the evaporator's upper surface. ΔT_{sub} is the subcooling of the inlet liquid while ΔT_{sup} is the superheating of the outlet vapor. L_{w-l} is the length of the wick-compensation cavity border. Since the natural convection heat transfer coefficient, h, at the evaporator's surface is very low, Q_h is negligible compared to the applied heat load. The inlet liquid velocity v_{in} can be expressed as follows:

$$v_{in} = \frac{qL_x}{\rho_l(L_x-L_{x3})(h_{fg}+c_l\Delta T_{sub}+c_v\Delta T_{sup})}. \tag{19}$$

According to the model of porous media saturated with fluid, the vapor-liquid interface is assumed to have zero thickness inside the wick structure and the liquid vapor transition is assumed to occur at the interface. Sharp discontinuities of the

fluid's properties appear across this interface, but continuities of the mass and heat flux should be maintained there.

Mass continuity condition:

$$\rho_l \vec{V}_l = \rho_v \vec{V}_v. \tag{20}$$

Energy conservation condition:

$$(k_{eff})_v \nabla T_v \cdot n - (k_{eff})_l \nabla T_l \cdot n = \rho_l |\vec{V}_l| h_{fg}. \tag{21}$$

Temperature continuity condition:

$$T_l = T_v = T_{sat}. \tag{22}$$

As evaporation takes place inside the wick structure, capillary menisci are established at the vapor-liquid interface. At the same time, capillary pressure develops, drawing the liquid through the wick to the vapor-liquid interface and circulating the fluid throughout the CPL:

$$\Delta P_c = P_v - P_l = \frac{2\sigma \cos\theta}{r_e}. \tag{23}$$

Equation (22) presents the local thermal equilibrium at the vapor-liquid interface inside the wick structure. The saturation temperature, T_{sat}, is equal to the setpoint temperature of the two-phase reservoir during normal operation of the CPL. This condition is used to determine the location of the vapor-liquid interface. As continuous flow of fluid is maintained by the capillary pressure in the wick, ΔP_c of Equation (23) should be equal to the total pressure loss of the entire CPL loop.

3. Numerical procedure

The governing equations and the boundary conditions for the various regions of the evaporator described above are solved as a conjugate problem with the SIMPLE algorithm, described in detailed in [11]. The conjugate problem includes liquid and vapor flow, heat transfer and phase change in the porous wick structure, liquid flow and heat transfer in the compensation cavity and heat transfer in the vapor grooves and the external metal wall, which increases the numerical procedure's complication significantly. An additional difficulty is the unknown location of the vapor-liquid interface involving a phase change. An interface tracking method based on a moving structured grid is used to locate the interface, regenerated at each step.

Under-relaxation and error feedback have been adopted in order to ensure convergence of the calculating procedure. The above-mentioned mathematical model can predict the evaporator's transient characteristics, but only the steady-state numerical results are discussed in this paper. The overall numerical sequence can be described as follows:

(1) initialize the problem and choose an initial arbitrary vapor-liquid location inside the wick;
(2) generate a structured grid in the region of $L_x \times L_{y3}$;
(3) solve the continuum and momentum equations separately in the $L_x \times L_{y3}$ region;
(4) regenerate the grid in the entire evaporator;
(5) solve the energy equations for all regions of the evaporator;

(6) check whether the temperature condition is satisfied at the interface. If negative, the vapor-liquid interface location has to be updated;
(7) go back to step (2) until convergence.

When the vapor-liquid interface is modified at step (6), a pressure drop across the interface is computed to ensure it is less than the maximum capillary pressure in the wick ($P_v - P_l \leq 2\sigma/r_e$). As the numerical technique for the solid zone of the computational domain when solving the continuum and momentum equations in the $L_x \times L_{y3}$ region has been described in detailed before (see [12]), it has not been repeated here.

The convergence criterion of the numerical solution for velocity, pressure and temperature is that relative errors between two consecutive iterations are less than 10^{-7}.

4. Results and discussions

Numerical results were obtained with ammonia as the working fluid. The following thermal properties were assumed in the computation: $k_l = 0.454\,\mathrm{W\,m^{-1}K^{-1}}$, $k_v = 0.0302\,\mathrm{W\ m^{-1}K^{-1}}$, $\mu_l = 2.0\cdot 10^{-4}\,\mathrm{Ns^{-1}m^{-2}}$, $\mu_v = 1.13\cdot 10^{-5}\,\mathrm{Ns^{-1}m^{-2}}$ and $h_f = 1.113\cdot 10^6\,\mathrm{Jkg^{-1}}$. A sintered stainless steel wick was used as the wick structure, with $k_s = 15.2\,\mathrm{W\,m^{-1}K^{-1}}$, $\varepsilon = 0.6$ and $K = 6.616\cdot 10^{-13}\,\mathrm{m^2}$. Aluminum ($k_{al} = 236\,\mathrm{W\,m^{-1}K^{-1}}$) and stainless steel ($k_{st} = 15.2\,\mathrm{W\,m^{-1}K^{-1}}$) were chosen as the materials of the metallic wall, since they are compatible with ammonia. The geometric parameters of the miniature flat-plate evaporator were as follows: $L_x = 10.5\cdot 10^{-3}\,\mathrm{m}$, $L_{x1} = 1.8\cdot 10^{-3}\,\mathrm{m}$, $L_{x2} = 2.4\cdot 10^{-3}\,\mathrm{m}$, $L_{x3} = 9\cdot 10^{-3}\,\mathrm{m}$, $L_y = 8\cdot 10^{-3}\,\mathrm{m}$, $L_{y1} = 1.8\cdot 10^{-3}\,\mathrm{m}$, $L_{y2} = 2.8\cdot 10^{-3}\,\mathrm{m}$ and $L_{y3} = 5.8\cdot 10^{-3}\,\mathrm{m}$. The length and height of vapor grooves were equal to $0.6\cdot 10^{-3}\,\mathrm{m}$. The setpoint temperature was 40°C, the liquid saturated temperature T_{sat}, and $\Delta T_{sub} = 10$°C. The grid schemes of the global evaporator are 107×82.

The velocity vectors for the liquid phase inside the evaporator with an aluminum wall at $q = 5\cdot 10^4\,\mathrm{W\,m^{-2}}$ are shown in Figure 4, the results for the liquid velocity profile in the compensation cavity being presented in Figure 4a. The velocity near the inlet is uniform along the flow direction, while the liquid's velocity decreases gradually as it makes its way down the compensation cavity, due to the mass reduction at the wick-compensation cavity interface. Because evaporation occurs mostly in the vicinity of the wick's upper surface, the liquid enters the wick from the compensation cavity nearly uniformly. The corresponding liquid velocity vectors inside the wick are shown in Figure 4b, the magnitude of liquid velocity being 10^{-5}. The wick structure includes a vapor region under the fins, separated from the liquid region by the vapor-liquid interface. The shape of the interface is wavy near the upper surface of the wick, and the vapor region is very small. The liquid flows into the wick from the wick-compensation cavity border and is made evaporate at the vapor-liquid interface by the wick capillary force. It is also evident from Figure 4b that evaporation mostly takes place in the vicinity of the upper wick surface, while the liquid's velocity is nearly uniform in most of the liquid zone. At the same time, because of the heat conduction effect of the metallic side wall, evaporation also occurs in the vicinity of

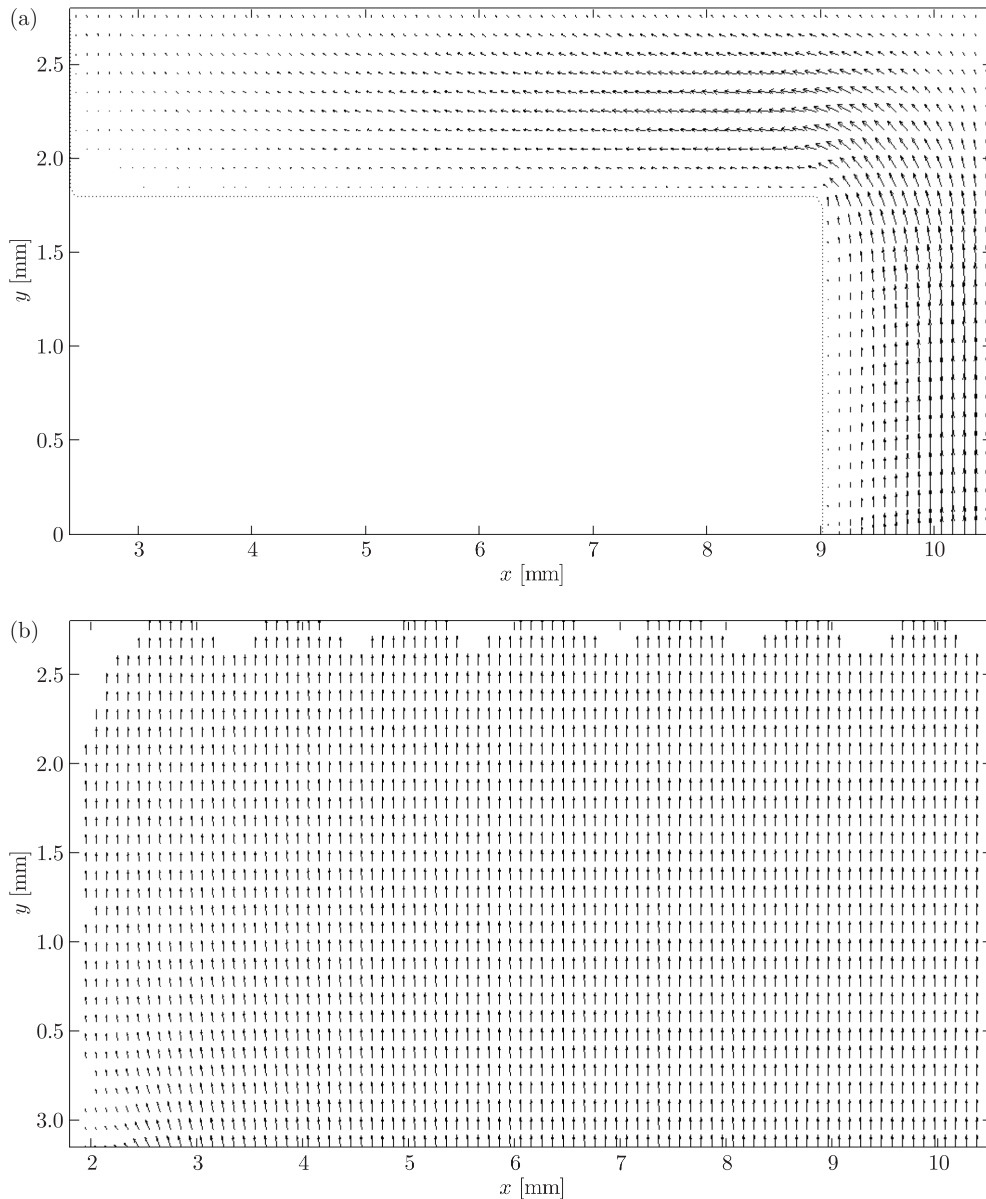

Figure 4. Liquid velocity vectors inside the evaporator:
(a) in the compensation cavity and (b) in the wick structure

the left-hand surface of the wick. Since the vapor zone is very small, the vapor velocity vectors are not given in this paper.

The temperature distributions of the evaporator with an aluminum wall are shown in Figure 5 for various heat fluxes. Because of the considerable difference in thermal conductivity between the metallic fins and the vapor, heat is transferred to the wick mainly by conduction of the fins, the shape of isotherms near the upper surface of the wick structure being wavy. The shape of the vapor-liquid interface, where the temperature contour level is equal to the saturated temperature inside the wick

(setpoint temperature of reservoir), is likewise wavy and determined by the geometric parameters of the fins and the vapor grooves. The vapor-liquid interface is located in the vicinity of the upper and left surfaces of the wick structure, as has been observed in the visualization experiment of Zhao *et al.* [13, 14]. Thin gaps appear between the fins and the upper surface of the wick saturated with vapor, allowing the vapor to escape from to the vapor grooves. When the heat flux is increased, the vapor-liquid interface inside the wick moves away from the fins and the vapor zone and the gaps increase in size. Due to the high thermal conductivity of aluminum, the temperature levels of the heated surface are very low and the temperature gradients inside the upper wall are very small, indicating that the temperatures of the evaporator's heated surface are almost isothermal.

As the thickness of the metallic side wall cannot be neglected for a miniature flat-plate evaporator, the effect of heat conduction of the metallic side wall on the heat transport capacity needs to be considered. As can be seen in Figure 5, the temperature of the bottom zone is higher than that of the middle zone of the compensation cavity, which indicates that the liquid in the compensation cavity has been heated significantly, due to the effect of heat conduction of the metallic side wall. At the heat flux of $q = 5 \cdot 10^4\,\mathrm{W\,m^{-2}}$, because k_{al} is much greater than k_s, the left vapor-liquid interface (40°C isotherm) inside the wick goes deeply into the left bottom surface of the wick, which means that evaporation occurs there and it is safe for CPL's normal operation. With increased heat flux, the influence of heat conduction of the metallic side wall on the vapor-liquid interface is very significant, as shown in Figure 5b. The 40°C isotherm has penetrated deeply into the bottom of the compensation cavity, indicating that vapor may be generated at the bottom of the compensation cavity. The presence of vapor in this area can block liquid flow to the vapor-liquid interface partially or fully, eventually resulting in the evaporator getting dry. For a miniature flat-plate CPL evaporator, if the thermal conductivity of the metallic wall exceeds the effective thermal conductivity of the wick, the effect of heat conduction of the metallic side wall leads to drying the evaporator. This is considered as a heat transfer limit, hereinafter referred to as the side wall effect heat transfer limit. Compared with other CPL heat transfer limits, it is a very important limit, with a great difference between a miniature flat-plate CPL and a cylindrical CPL.

Due to the existence of the side wall effect heat transfer limit, a capillary evaporator with an aluminum wall has low heat transport capability and is not suitable for dissipating high heat fluxes in electronic devices. In order to improve the heat transfer limit, wall materials of lower thermal conductivity should be chosen, such as stainless steel. The temperature profiles of an evaporator with a stainless steel wall and various heat fluxes are shown in Figure 6. Because stainless steel's low thermal conductivity, the temperature gradient is very high in the upper wall zone and decreases inside the wick. Apparently, most of applied heat load is used for evaporation near the upper and left surfaces of the wick. The liquid in the compensation cavity is heated, but the effect of heat conduction of the metallic side wall is limited by the high thermal resistance of the side wall. The vapor-liquid interface extends to the left bottom surface of wick only and does not penetrate deeply into the bottom interface of the compensation cavity, which indicates that the CPL can operate safely even at

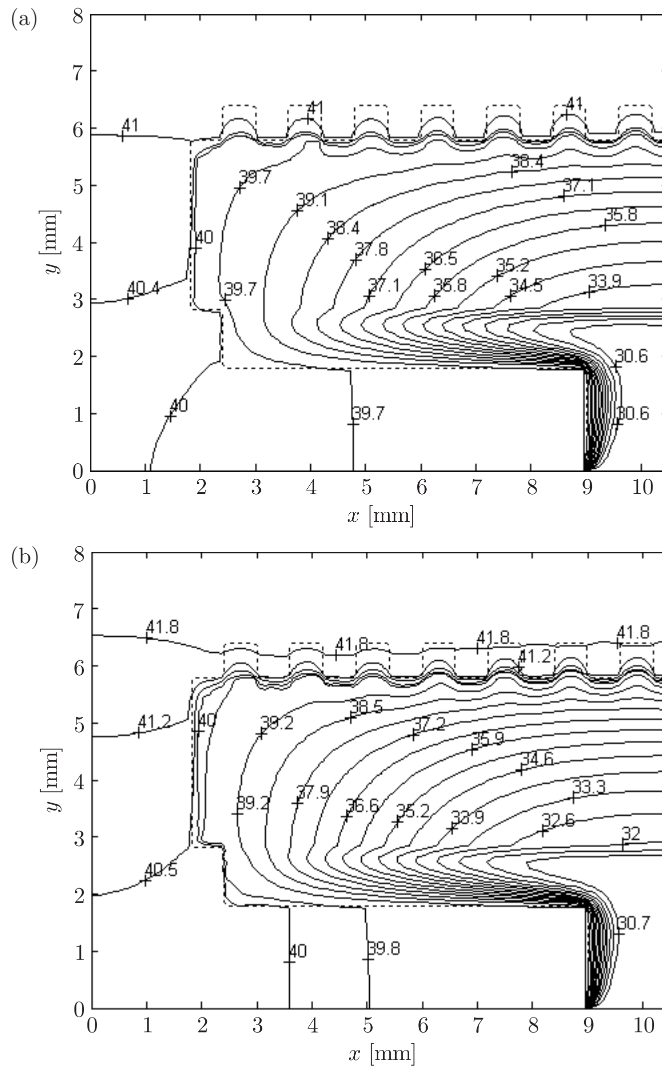

Figure 5. Temperature fields in the evaporator with an aluminum wall: (a) $q = 5 \cdot 10^4\,\mathrm{W m^{-2}}$ and (b) $q = 7.5 \cdot 10^4\,\mathrm{W m^{-2}}$

$q = 15 \cdot 10^4\,\mathrm{W m^{-2}}$. As a result, a flat plate evaporator with a stainless steel wall has a high side wall effect heat transfer limit, implying that an evaporator with a wall of low thermal conductivity can dissipate high heat fluxes.

As the evaporator's heated surface is directly attached to the electronic apparatus, high temperatures of the heated surface may result in its abnormal operation. Therefore, the purpose of CPL's electronic in cooling applications is to maintain the junction temperature below a safety limit by pumping heat away from electronic devices. Another key performance parameter of any high-flux electronic cooling scheme is the ability to maintain a fairly isothermal device surface [15]. Temperature profiles along the heated surface of an evaporator with a stainless steel wall are shown in Figure 7 for various heat fluxes applied. The temperature of the heated surface increases with the applied heat fluxes as expected and decreases along the x direc-

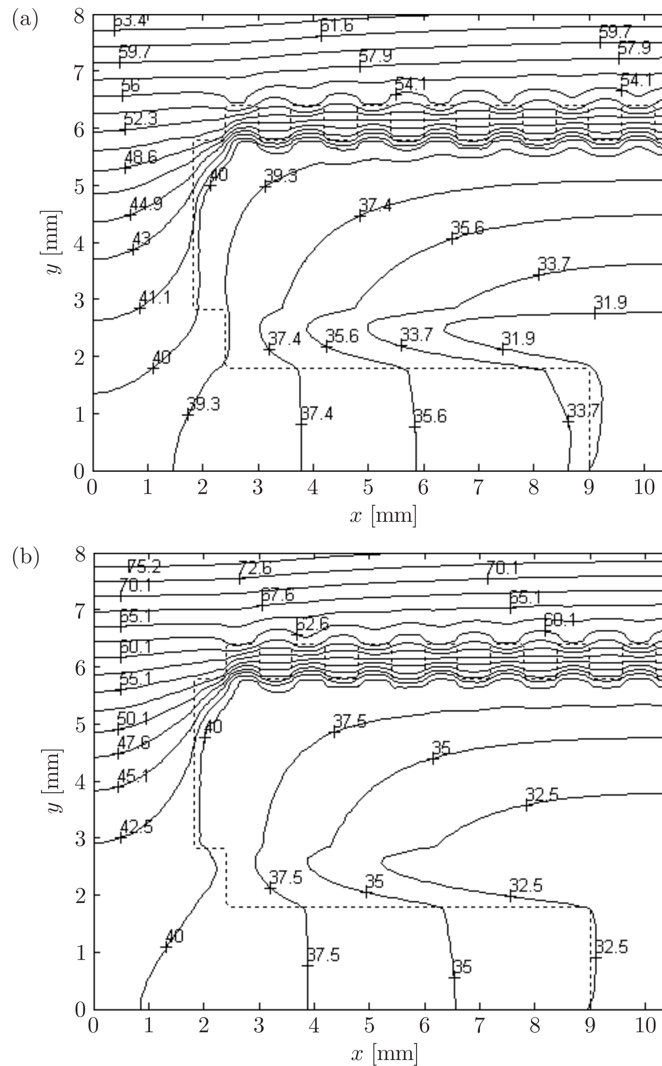

Figure 6. Temperature fields in the evaporator with a stainless steel wall: (a) $q = 10 \cdot 10^4\,\mathrm{W\,m^{-2}}$ and (b) $q = 15 \cdot 10^4\,\mathrm{W\,m^{-2}}$

tion. Due to the high thermal resistance of the stainless steel wall, the temperature level of the heated surface is very high, the maximum temperature exceeding 77°C at $q = 15 \cdot 10^4\,\mathrm{W\,m^{-2}}$, which is a great disadvantage for electronic cooling applications. At the same time, the temperature difference along the heated surface increases with the heat load, the maximum temperature difference exceeding 3.5°C at $q = 15 \cdot 10^4\,\mathrm{W\,m^{-2}}$, which implies that the isothermal characteristic of the heated surface is not very well. An evaporator with a stainless steel wall is capable of dissipating high heat flux, but cannot maintain low surface temperatures and a desirable isothermal surface. In order to deal with these problems, a capillary evaporator for electronic cooling applications should be designed with combined walls: the upper wall of a high thermal conductivity material, the side and bottom walls of a low thermal conductivity material.

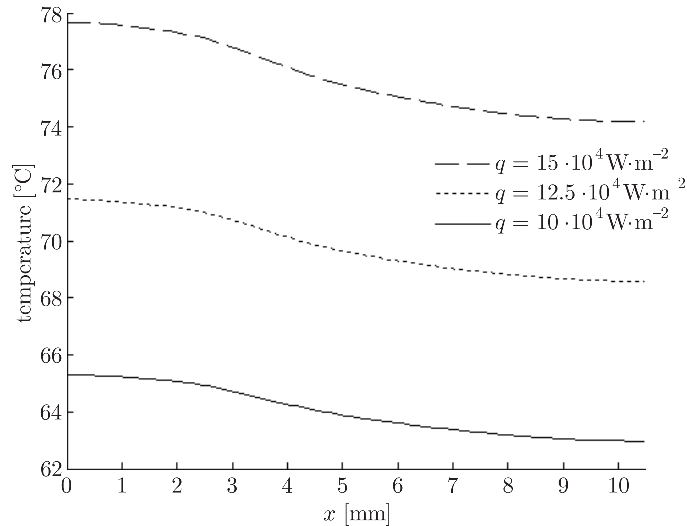

Figure 7. Temperature distributions at the evaporator's heated surface

Temperature distributions in an evaporator with combined walls (the upper wall's material being aluminum, the side and bottom walls' material being stainless steel) at various heat fluxes are shown in Figure 8. Due to the high thermal conductivity of the upper wall, temperature gradients are small in that zone and high inside the wick and in the side and bottom walls. The effect of heat conduction of the side wall is obviously weaker and, even at $q = 15 \cdot 10^4\,\mathrm{W m^{-2}}$, the left vapor-liquid interface is located near the center of the wick's left surface, which indicates that the CPL has not reached the side wall effect heat transfer limit and can operate safely.

Temperature distributions of the heated surface of an evaporator with a combined wall are shown in Figure 9 for various heat fluxes. The temperature of the heated surface is moderate, even at $q = 17.5 \cdot 10^4\,\mathrm{W m^{-2}}$, the maximum temperature being about 50.3°C and the maximum temperature difference around 2°C, which indicates that the electronic device can operate effectively and enjoy a long operating life. A flat-plate evaporator with combined walls can effectively improve heat transport capacity and maintain an appropriate temperature level of the heated surface.

5. Conclusions

A two-dimensional model of a global evaporator of a miniature flat capillary pumped loop has been developed to describe heat and mass transfer in the porous wick structure and heat transfer in the fluid region and the external metal wall. Governing equations for the different zones have been solved numerically as a conjugate problem using the SIMPLE algorithm.

The location and shape of the vapor-liquid interface are mainly affected by the heat load and geometric parameters of fins and vapor grooves. Evaporation takes place near the upper and left surfaces of the wick structure. As the effect of heat conduction of the metallic side wall on the miniature flat-plate CPL evaporator's behavior is considerable, a side wall effect heat transfer limit has been introduced to

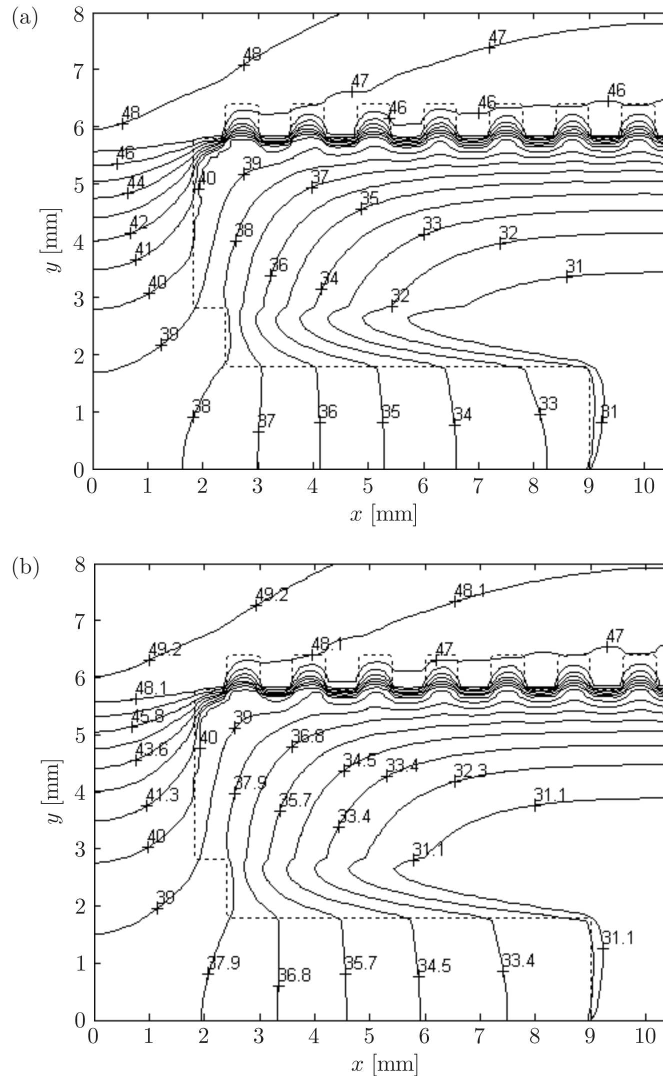

Figure 8. Temperature fields in the evaporator with combined walls: (a) $q = 15 \cdot 10^4\,\mathrm{Wm^{-2}}$ and (b) $q = 17.5 \cdot 10^4\,\mathrm{Wm^{-2}}$

estimate the evaporator's performance. Due to its existence, an evaporator with an aluminum wall has low heat transport capacity but leads to lower temperatures and good isothermal behavior of the heated surface. An evaporator with a single stainless steel wall has higher heat transport capacity but higher temperatures of the heated surface. An evaporator with combined walls (the upper wall of aluminum, the side and bottom walls of stainless steel) can significantly increase the side wall effect heat transfer limit and maintain an appropriate temperature level and a good isothermal characteristic on the heated surface, so that the CPL can operate safely and the electronic device can work effectively at higher heat fluxes.

The present overall numerical model of a miniature flat-plate CPL evaporator can effectively estimate the heat transfer capacity of an evaporator and evaluate the

tq112a-e/18 30 IX 2008 BOP s.c., http://www.bop.com.pl

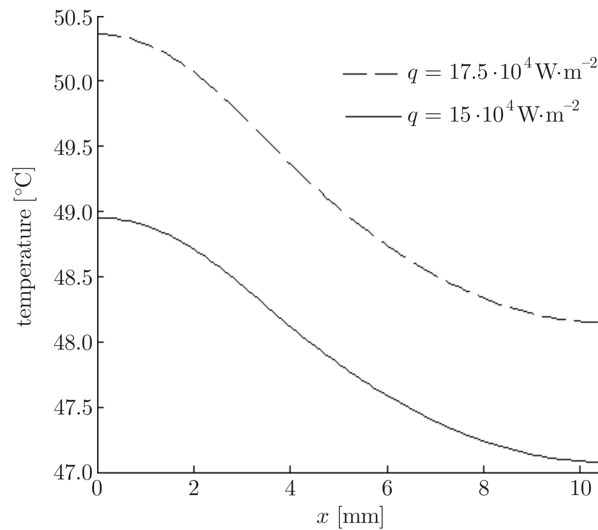

Figure 9. Temperature profiles along the heated surface

temperature level of the heated surface, thus being helpful in the evaporator design and optimization of miniature flat-plate CPL's.

Acknowledgements

The present work has been supported by the National Key Basic Research Development Program of China (No. 2007CB206901).

References

[1] McGlen R J, Jachuck R and Lin S 2004 *Appl. Thermal Engng* **24** (8) 1143
[2] Garimella S V 2006 *Microelectronics J.* **37** (11) 1165
[3] Riehl R R and Dutra T 2005 *Appl. Thermal Engng* **25** (1) 101
[4] Pouzet E, Joly J L, Platel V, Grandpeix J-Y and Butto C 2004 *Int. J. Heat and Mass Transfer* **47** (10–11) 2293
[5] Nadalini R and Bodendieck F 2006 *Acta Astronautica* **58** (11) 564
[6] Cao Y and Faghri A 1994 *Int. J. Heat and Mass Transfer* **37** (10) 1525
[7] Demidov A S and Yatsenko E S 1994 *Int. J. Heat Mass Transfer* **37** (14) 2155
[8] Figus C, Bray Y Le, Bories S and Prat M 1999 *Int. J. Heat Mass Transfer* **42** (14) 2557
[9] Yan Y H and Ochterbeck J M 2003 *J. Electronic Packaging* **125** (2) 251
[10] Clair T J La and Mudawar I 2000 *Int. J. Heat and Mass Transfer* **43** (21) 3937
[11] Patankar S 1980 *Numerical Heat Transfer and Fluid Flow*, Mcgraw-Hill, New York
[12] Yang M and Tao W Q 1995 *ASME J. Heat Transfer* **117** 619
[13] Zhao T S and Liao Q 2000 *Int. J. Heat and Mass Transfer* **43** (7) 1141
[14] Zhao T S, Cheng P and Wang C Y 2000 *Chem. Engng Sci.* **55** (14) 2653
[15] Meyer M T, Mudawar I, Boyack Ch E and Hale Ch A (2006) *Int. J. Heat and Mass Transfer* **49** (1–2) 17